

Electronic and structural properties of superconducting MgB_2 , CaSi_2 and related compounds

G. Satta[†], G. Profeta^{*}, F. Bernardini[†], A. Continenza^{*} and S. Massidda[†]

^{}Istituto Nazionale di Fisica della Materia (INFM) and Dipartimento di Fisica, Università degli Studi di L'Aquila, I-67010 Coppito (L'Aquila), Italy*

[†]Istituto Nazionale di Fisica della Materia (INFM) and Dipartimento di Fisica Università degli Studi di Cagliari, 09124 Cagliari, Italy

Abstract

We report a detailed study of the electronic and structural properties of the 39K superconductor MgB_2 and of several related systems of the same family, namely $\text{Mg}_{0.5}\text{Al}_{0.5}\text{B}_2$, BeB_2 , CaSi_2 and CaBeSi . Our calculations, which include zone-center phonon frequencies and transport properties, are performed within the local density approximation to the density functional theory, using the full-potential linearized augmented plane wave (FLAPW) and the norm-conserving pseudopotential methods. Our results indicate essentially three-dimensional properties for these compounds; however, strongly two-dimensional σ -bonding bands contribute significantly at the Fermi level. Similarities and differences between MgB_2 and BeB_2 (whose superconducting properties have not been yet investigated) are analyzed in detail. Our calculations for $\text{Mg}_{0.5}\text{Al}_{0.5}\text{B}_2$ show that metal substitution cannot be fully described in a rigid band model. CaSi_2 is studied as a function of pressure, and Be substitution in the Si planes leads to a stable compound similar in many aspects to diborides.

PACS numbers: 74.25.jb, 74.70.-b, 74.10.+v, 71.20.-b

Typeset using REVTeX

I. INTRODUCTION

The recent discovery [1] of superconductivity at $\approx 39\text{K}$ in the simple intermetallic compound MgB_2 is particularly interesting for many reasons. In the first instance, this critical temperature is by far the highest if we exclude oxides and C_{60} based materials. Furthermore, B isotope effect [2] suggests that MgB_2 is a BCS phonon-mediated superconductor, with T_c above the commonly accepted limits for phonon-assisted superconductivity. Another reason of interest is that the AlB_2 -type structure of MgB_2 (which can be viewed as an intercalated graphite structure with full occupation of interstitial sites centered in hexagonal prisms made of B atoms) is shared by a large class of compounds (more than one hundred), where the B site can be occupied by Si or Ge, but also by Ni, Ga, Cu, Ag, Au, Zn and Cd, and Mg can be substituted by divalent or trivalent *sp* metals, transition elements or rare earths. Such a variety is therefore particularly suggestive of a systematic study of diborides and structurally related compounds. To confirm this interest, a recent study [3] showed that superconductivity is suppressed by addition of more than about 30% of Al atoms. Pressure effects [4] also lead to a depression of superconductivity.

Early studies [5–7] of the electronic structure of diborides by the OPW and tight-binding methods have shown similarity with graphite bands. A more systematic study of AlB_2 -type compounds [8,9] by the full-potential LAPW method showed in simple metal diborides the presence of interlayer states, similar to those previously found in graphite [10,11], in addition to graphite-like σ and π bands. Transition metal diborides, on the other hand, show a more complex band structure due to the metal *d* states. A very recent electronic structure calculation [12] on MgB_2 shows that metallicity is due to B states. Phonon frequencies and electron-phonon couplings (at the Γ point) lead these authors to suggest phonon-based superconductivity. Further, new calculations [13] on related compounds (LiB₂ and graphitic-like B) addressed the peculiar contributions to conductivity coming from the interplay of 2D and 3D Fermi surface features. An alternative mechanism has been proposed by Hirsch [14], based on dressed hole carriers in the B planes, in the presence of almost filled bands.

Recently, superconductivity at $T_c \approx 14\text{K}$ was observed in CaSi_2 [15]. In this compound, high pressure has been effectively used to tune both structural and physical properties [15,16]. In particular, Bordet and co-workers [15] identified a new structural phase transition for CaSi_2 from trigonal to hexagonal AlB_2 -type structure, with superconductivity at $T_c = 14\text{ K}$, one of the highest transition temperatures known for a silicon based compound. The occurrence of this structural phase transition indicates that Si shifts from an sp^3 to an sp^2 -like hybridization, and experiment points to a clear enhancement of T_c with high pressure [15]. Many electronic structure studies have been carried out for the different phases [17–19] of disilicides. CaSi_2 in the AlB_2 structure was studied by Kusakabe et al. [20], but a final answer on the stability of this phase under pressure is still lacking.

As previously pointed out, the AlB_2 family of compounds provides a wide playground for the search of new superconductors, and we intend to provide here a contribution, based on a detailed study of electronic and structural properties together with phonon spectra, for several diborides and for CaSi_2 , in the trigonal and hexagonal structures. The questions that we want to address are the following: (i) how do the electronic properties of MX_2 depend on the atomic species M; namely, can rigid band schemes provide the correct trend, or is the metal effect mostly mediated by lattice parameter changes (chemical pressure). (ii) Ref. [12] shows the presence of both B π Fermi surfaces (FS) giving rise to 3-dimensional states, and of small 2-dimensional B σ -bonding pockets. It is of course interesting to know which of the FS is mostly involved in superconductivity. The trends observed in the band structures, together with experimental studies, will contribute to elucidate this point. In the same way, changes in the Fermi level density of states with chemical composition will possibly correlate with T_c values. (iii) Pure CaSi_2 shows a trigonal instability, joined by a buckling of Si_2 planes, which is apparently [15] strongly reduced under high pressure, or by Be substituting some of the Si sites. The presence, or the proximity, of structural instabilities (investigated through phonon spectra), will hopefully provide hints to further experimental search for new materials.

In this paper, we present calculations for MgB_2 , $\text{Mg}_{0.5}\text{Al}_{0.5}\text{B}_2$, BeB_2 , CaSi_2 and

CaBe_xSi_{2-x} ($x = 1$), based on the local density approximation (LDA) to the density functional theory. We use both the Full Linearized Augmented Plane Wave method, and the norm-conserving pseudopotential method. In Sect. II we give some computational detail; in Sect. III and IV we discuss the electronic properties for all the compounds considered; we finally draw our conclusion in Sect. V.

II. COMPUTATIONAL AND STRUCTURAL DETAILS

Our calculations were performed using the “all-electron” full potential linearized augmented plane waves (FLAPW) [21] method, in the local density approximation (LDA) to the density functional theory. In the interstitial region we used plane waves with wave vector up to $K_{max} = 3.9$ a.u. and 4.1 a.u. for disilicides and diborides, respectively (we used the larger $K_{max} = 4.4$ a.u. for BeB₂ because of the smaller spheres imposed by the smaller lattice parameters). Inside the muffin tin spheres, we used an angular momentum expansion up to $l_{max} = 6$ for the potential and charge density and $l_{max} = 8$ for the wave functions. The Brillouin zone sampling was performed using the special k -points technique according to the Monkhorst-Pack scheme [22], and also the linear tetrahedron method with up to 120 k -points in the irreducible Brillouin zone. We used muffin tin radii $R_{MT} = 2.2, 1.8, 1.59$ and 2.1 a.u., for Ca, Si, B, and the remaining elements respectively (we used $R_{Be} = 2$ a.u. and $R_B = 1.5$ a.u. in BeB₂).

The crystallographic structure of AlB₂ (C32) is hexagonal, space group $P6mmm$ with graphitic B planes, and 12-fold B-coordinated Al atoms sitting at the center of B hexagonal prisms. The unit cell contains one formula unit, with Al atom at the origin of the coordinates and two B atoms in the positions ($\mathbf{d}_1 = (a/2, a/2\sqrt{3}, c/2)$, $\mathbf{d}_2 = -\mathbf{d}_1$). The trigonal distortion in CaSi₂ corresponds to a buckling of Si planes leading to a $P3\bar{m}1$ space group symmetry), with one internal structural parameter z (the internal coordinate of B atoms).

To calculate plasma frequencies, Fermi velocities, Hall coefficients, and the densities of states (DOS) near E_F , we have performed a spline fit [23] of the *ab-initio* energy bands.

The fitted bands have then been computed over 128^3 points in the reciprocal space unit cell. The linear tetrahedron method has been used to compute DOS and the other quantities.

Phonon frequencies were computed using the ABINIT code [24] by means of Linear Response Theory [25,26] (LRT) approach in the framework of pseudopotentials plane wave method [24]. Troullier and Martins [27] soft norm-conserving pseudopotentials were used for all the elements considered, Mg and Ca p semicore states were not included in the valence, their contribution to the exchange and correlation potential was accounted by the non-linear core corrections [28]. The local density approximation to the exchange-correlation functional is used. Plane wave cutoffs of 44 Ry and 30 Ry were found sufficient to converge structural and electronic properties of the diborides and silicides respectively. Brillouin zone integration was performed using a $20 \times 20 \times 20$ Monkhorst-Pack [22] mesh for the structural optimization and a $12 \times 12 \times 12$ mesh was used in the LRT selfconsistent calculation of phonon frequencies. To improve k -point sampling convergence a gaussian smearing with an electronic temperature of 0.005 Ha was used. The structure used in the LRT calculations was obtained optimizing the lattice structure up to a residual stress of 1 MPa.

III. DIBORIDES

A. MgB₂ and BeB₂.

We shall start our discussion of electronic properties of diborides by presenting in Fig. 1 the energy bands of the superconducting compound MgB₂, which will be the reference for all our further studies (the $M - \Gamma - K$ lines are in the basal plane, while the $L - A - H$ lines are the corresponding ones on the top plane at $k_z = \pi/c$). We used the experimental lattice parameters $a = 3.083 \text{ \AA}$, $c = 3.52 \text{ \AA}$. Our results, which are in excellent agreement with those of Kortus et. al. [12], show strong similarities with the band structures of most simple-metal diborides [8], computed by the FLAPW method. They show strongly bonded sp^2 hybrids laying in the horizontal hexagonal planes, forming the three lowest (σ -bonding) bands, as

the main structure in the valence region. The corresponding antibonding combinations are located around 6 eV above the Fermi level (E_F).

The bonding along the vertical direction is provided by the π bands (at ~ -3 eV and ~ 2 at Γ), forming the double bell-shaped structures. Similarly to AlB₂-type diborides, and unlike graphite, we notice a large dispersion of the π bands along the k_z direction ($\Gamma - A$). This can be understood on a tight-binding approach: the phases of the Bloch functions lead the B p_z orbitals on adjacent layers to be antibonding at Γ , and bonding at A . The downwards dispersion of the π -bonding band (from -3 to -7 eV along $\Gamma - A$) is joined by an opposite upwards dispersion of an empty band, (at ≈ 2 eV at the Γ point). The analysis of the wavefunctions for this empty band reveals that this band has an interstitial character, and is very similar to those found in graphite [11], in diborides [8], in CaGa₂ [9], but also in CaSi₂. A general description of the bonding can be given by the partial density of states (PDOS), shown in Fig. 2. The B PDOS, in particular, shows bonding and antibonding structures for the s and p states. The p_z states give rise to a rather wide structure responsible for less than half of the DOS at E_F , which therefore results having predominantly B $p - \sigma$ character.

In the search of similar materials having the desired superconducting properties, BeB₂ is the first natural candidate, as the band filling is expected to be pretty similar, and lighter Be atoms may help providing larger phonon frequencies while keeping similar electronic properties. The first experimental report on BeB₂ [29] gives the average lattice constants. These experimental parameters have been used for all the previous calculations of the BeB₂ [6,8]. We have optimized the lattice constants, imposing the AlB₂ structure, obtaining $a = 2.87\text{\AA}$, $c = 2.85\text{\AA}$, smaller than in MgB₂ and similar to the values estimated by the average experimental values. In particular, we notice that while a reduces only by about 7.4%, c reduces by about 24% when Mg is substituted by Be, a result which can be understood pretty easily. On one hand, in fact, the optimization of σ -bonds prevents a too drastic variation of the a parameter; on the other hand, c can change more easily as the vertical bonding, provided by the π bands, has a large contribution from the metal orbitals. The

band structure of BeB₂, shown in Fig 3, are pretty similar to those computed by the FLAPW method [8] at the experimentally estimated lattice parameters. We can remark the strong similarities with the MgB₂ compound, which includes the presence of σ -bonding hole pockets along $\Gamma - A$, but also a few relevant differences. First of all, the shorter lattice parameters lead to wider valence bands, and also to more dispersed σ bands, in particular the cylindrical hole pocket along $\Gamma - A$, which might be relevant for superconductivity. Also, the different energy location of the metal s -free electron band (lower in MgB₂), and the different shape of the π -bonding band (related by the different c values) causes a different occupation of this band, especially along $\Gamma - M$.

To further investigate these two materials, and their relation to isostructural diborides, we studied the zone center phonon frequencies of MgB₂, BeB₂, and AlB₂, using the linear response approach, with the pseudopotential method. The calculations have been carried out at the theoretical lattice constants (also listed in Table I), as obtained using the same method. The two lowest independent frequencies correspond to a motion of the intercalated metal atoms relative to the rigid B networks: one vertical mode (A_{2u}), and one doubly degenerate in-plane mode, (E_{1u}). The two higher frequencies represent the internal motion of the B network itself: again one vertical mode (B_{1g}), now representing a trigonal distortion producing a buckling of the planes similar to that found in CaSi₂, and one degenerate (E_{2g}) mode giving an in-plane stretching of B-B bonds. Our calculations for MgB₂ are in good with other results [12,30]. The comparison between the MgB₂ and BeB₂ shows a much higher E_{2g} frequency in BeB₂. This result cannot be explained through the different atomic masses, as it involves only B motion. It is therefore related to the different coupling of the electrons with the nuclear system. Surprisingly, two of the remaining frequencies are lower in BeB₂, namely the A_{2u} mode which involves the motion of lighter Be atoms against the B network and the B_{1g} mode. This indicates a strong dependence of the phonon spectra of these materials on the electronic structure details. The lowest E_{1u} mode has comparable frequencies. If we now go to AlB₂, we see again that the E_{2g} mode is much higher than in MgB₂. Therefore, this mode has his minimum value in the superconducting material. The

modes involving the relative motion of the B_2 planes as a whole have frequencies comparable to the other materials; the B_{1g} , on the other hand, is smaller than in MgB_2 and BeB_2 , which is probably a consequence of the larger band filling (see the discussion on $CaSi_2$ below).

We have computed, within a rigid band scheme and using the scheme described, e.g., in Ref. [23], the Fermi velocities, plasma frequencies (along the principal axes of the crystal), and the independent components of the Hall tensor for BeB_2 and MgB_2 . Because of hexagonal symmetry, the non-zero components will be R_{xyz} , corresponding to the magnetic field along the z axis and transport in plane, and $R_{zxy} = R_{yzx}$ corresponding to in-plane magnetic field. The results, plotted in Fig. 4 as a function of the hole or electron-type doping, show relatively smooth variations over a wide range of doping, and are nearly coinciding, at zero doping, with the corresponding calculations by Kortus et al. [12]. After comparing the two materials, the following remarks can be done: (i) the density of states at E_F is smaller in BeB_2 . (ii) MgB_2 is nearly isotropic in terms of plasma frequencies and Fermi velocities, while BeB_2 is expected to show important anisotropy in resistivity, and, in particular, the in-plane conductivity is expected to be smaller. A band-by-band decomposition explains these results in term of very similar (and very anisotropic) contributions in the two compounds from σ states, and quite different contributions from the π bands, nearly isotropic in MgB_2 and favoring conductivity along the c -axis in BeB_2 . These results point out that despite structural similarity, the electronic properties of AlB_2 -type structures differ substantially from graphite and intercalation graphite compounds. (iii) The Hall coefficients are positive (hole-like) when the magnetic field is along the z axis (transport in-plane), while is negative for MgB_2 and almost zero but negative for BeB_2 , when the magnetic field is in-plane. A detailed analysis shows again comparable contributions in the two compounds from σ bands, while the sign of R_{zxy} and R_{yzx} comes from a balance of the π bands. The Hall coefficient of MgB_2 has been recently measured by Kang et al. [31]. R_H , which will correspond in this case to an average of the tensor components, turns out to be positive and to decrease with temperature. At $T = 100K$ they give $R_H = 4.1 \times 10^{-11} m^3/C$, and an extrapolation of their results at $T \rightarrow 0$, gives $R_H \approx 6.5 \times 10^{-11} m^3/C$. If we average, at

zero doping, our tensor components, the positive contributions overcome the negative ones, resulting in an average value $R_H \approx 2 \times 10^{-11} \text{m}^3/\text{C}$. This value is thus of the correct order, but single crystal measurements are probably necessary to have a significant comparison, avoiding an average of quantities with different sign. It is worth noticing that, if the sign of carriers has a role on superconductivity [14], BeB₂ also has a positive Hall coefficient.

B. Al doping in MgB₂.

A recent experimental report by Slusky et al. [3] shows that Al doping destroys bulk superconductivity when the Al content x is greater than ≈ 0.3 . Stimulated by these results, we studied the chemical substitution of Mg with Al. The substitution corresponding to a 50% concentration of Al ($x = 0.5$) leads to a reduction of the cell parameters, from $a = 3.083 \text{ \AA}$, $c = 3.521 \text{ \AA}$ [32] for MgB₂, to $a = 3.047 \text{ \AA}$, $c = 3.366 \text{ \AA}$ [32] for Mg_{0.5}Al_{0.5}B₂. These differences again indicate hardly compressible B-B σ bonds, and interlayer distances quite sensitive to the intercalated cation. The study of Slusky et al. [3] shows consistent results, and indicates, furthermore, that after a two-phases region for Al substitutions from 10 to 25%, c collapses and bulk superconductivity disappears. We first studied this problem in a rigid band approach, bringing MgB₂ to the same lattice parameters of Al_{0.3}Mg_{0.7}B₂ [3]. The only apparent change at that electron concentration is the complete filling of the π bonding band at the M point. The σ bonding bands need a larger electron addition to be completely filled in a rigid band model.

To investigate further this problem, we studied the system with 50% Al concentration. We used in our calculations the experimental values, and in a first approach simulated the disorder (certainly present in the real compound) using an orthorhombic supercell. The corresponding unit cell contains two formula units, and is described by the two orthogonal in plane basis vectors $\mathbf{a}_1 = (a, 0, 0)$ and $\mathbf{a}_2 = (0, a\sqrt{3}, 0)$. We started by calculating the energy bands using the MgB₂ lattice constants, and then we used the experimental Mg_{0.5}Al_{0.5}B₂ constants. The results of these calculations are shown in Fig. 5 together with the bands of

MgB₂, folded into the Brillouin zone (BZ) of the orthorhombic structure. The folding is such that the Γ point of the orthorhombic BZ corresponds to the Γ and M points of the hexagonal BZ, while Z corresponds to both the hexagonal A and L . Therefore, the $\Gamma - Z$ line collects the $\Gamma - A$ and the $M - L$ hexagonal lines, and we notice immediately the three π bands (two bonding and one anti-bonding, coming from folding). The $\Gamma - X$ line contains the (folded) hexagonal $\Gamma - M$ line. If we first look at the frozen structure calculation Fig. 5(c), we see quite similar band dispersions with the obvious splittings, related to the symmetry lowering induced by the different cations, and a different band filling. We notice, however, a lowering of the folded π antibonding band, related to the different cations: the π band is in fact pushed downwards by the interaction with the free-electron metal- s band, which is at lower energy in the compounds with Al (this band is partially filled in pure, non superconducting, AlB₂ [8]). As a consequence, the extra electrons coming from Al do not fill the σ -bonding band completely, leaving hole pockets around Z . As we relax the structure, the σ bands increase their width due to the smaller a value, and the situation near E_F changes only because of the occupation of the free-electron band around Γ . These results suggest that although the rigid band scheme can be considered roughly correct, the dependence upon doping of the physical properties and of Fermi surface states relevant for superconductivity, may be crucially dependent on the actual substitutional atom.

IV. CaSi₂ AND RELATED COMPOUNDS

When prepared at ambient pressure CaSi₂ has a rhombohedral structure (space group $R\bar{3}m$, $a = 3.85 \text{ \AA}$, $c = 30.62 \text{ \AA}$) [33] and is a semimetal [18], not superconducting down to 30 mK [34]. By annealing under pressure - typical conditions are 8 GPa and 800 K - a tetragonal superconducting (α - ThSi₂ - type) phase appears with a 3-dimensional network [35] of Si, showing superconductivity with $T_c = 1.58 \text{ K}$. At pressures between $\approx 7 \text{ GPa}$ and 9.5 GPa , rhombohedral structure samples undergo a transition to a trigonal phase ($P\bar{3}m1$, $a_T \approx 3.78 \text{ \AA}$, $c_T \approx c_R/6 \approx 4.59 \text{ \AA}$) with Si at $2d$ positions, and $z = 0.4$, where z is the

coordinate of the B atoms in units of c ($z = 0.5$ corresponds to the perfect AlB_2 structure). A second phase transition occurs at 16 GPa. This new phase may be described as [15] an AlB_2 -like structure with z slightly smaller than the ideal value $1/2$. The AlB_2 -type structure was previously observed in rare-earth silicides [36], while in CaSi_2 it is apparently stabilized by doping the Si planes with Be [37].

In Fig. 6 we show the energy bands of CaSi_2 in the AlB_2 structure (dashed lines), superimposed with those of the trigonal structure (full lines), along the main symmetry lines of the Brillouin zone. Since this polymorph can be obtained only under pressure, we do not minimize the lattice parameters, but rather use the experimental values $a = 3.7077 \text{ \AA}$ and $c = 4.0277 \text{ \AA}$, corresponding to $P=19.3 \text{ GPa}$, and optimize the internal parameter z . The bands in the AlB_2 structure show strong similarities with those of simple metal diborides, and of CaGa_2 [8]. The major difference is provided by Ca d states, which are mostly found in the conduction region, above 4 eV; however, there is a p - d mixing between Si and Ca, especially concerning Si π and Ca d_{z^2} orbitals, also mixing with the free-electron states. Unlike in MgB_2 , the Fermi level of CaSi_2 cuts only the antibonding part of the π bands, while the bonding part is fully occupied. This of course implies a reduced contribution of π states to the stabilization of an sp^2 environment, consistent with the sp^3 -like trigonal distortion. We will come back to this point later. The energy bands in the trigonal structure show that, apart from a small rigid shift, the σ bands change very little with respect to the AlB_2 structure. The π bands, on the other hand, show anticrossings which in the antibonding case are located right at the Fermi level. This is most clearly indicated in the density of states of CaSi_2 , reported in Fig. 7. The dip at E_F in the trigonal structure provides a textbook explanation for the lattice distortion.

In order to understand the stability of AlB_2 -type polymorph, we study the total energy variation as a function of z , relative to the ideal $z = 0.5$ case, for two experimental structures [15], and report it in Fig. 8(a). There is a good agreement between theory and experiment (within 2.5%), and a non-negligible ($\approx 30 \text{ mRy}$ per formula unit) stabilization energy. We notice, however, that the stabilization energy decreases with pressure. As we fix a and c to

the values corresponding to the larger pressure of 19.3 GPa [15], we see a larger discrepancy relative to the experimental equilibrium value of z ($z_{exp} \sim 0.448$). This indicates that some different modification might be going on in the experimental samples. In order to discuss the link between the stability of CaSi_2 in the AlB_2 structure and the π -band filling, without modifying the Si_2 planes themselves, we vary the atomic number of the cation, which now represents a virtual atom ranging from Ca to K (corresponding to $Z = 20 + x$). Our results, reported in Fig 8(b), show that while $x = -0.3$ leaves the total energy curve almost unchanged, $x = -0.7$ or larger give a nearly vanishing trigonal stabilization energy. This is consistent with our previous conclusion that a filling of π -antibonding bands destabilizes the AlB_2 structure.

This last conclusion is supported by the existence, in the hexagonal structure, of $\text{CaBe}_x\text{Si}_{2-x}$, with $x = 0.75$, at $a = 3.94 \text{ \AA}$ and $c = 4.38 \text{ \AA}$ [37]. In fact, Be doping removes electrons from the Si_2 planes, and brings the formal filling of the above π -antibonding bands to the level found in diborides. To investigate these effects, we studied the (artificially ordered, but existing) $\text{CaBe}_x\text{Si}_{2-x}$ system for $x = 1$, not far from the experimental stoichiometry. The corresponding bands, shown in Fig. 9, have been calculated at the experimental lattice parameters ordering Be and Si atoms as, e.g., in hexagonal BN. In this way, the Brillouin zone is the same as in the undoped compound, and the interpretation is easier. The CaBeSi band structure shown are overall similar to that of the undoped compound. The symmetry lowering induced by substitution produces the large splitting of degeneracies at the K and H points. The major difference is of course related to the position of the Fermi level, which is almost exactly coinciding with that found in the superconducting MgB_2 . The reduced bandwidth for the σ bonding bands may be associated with the smaller size of Be orbitals. The electron depletion from the antibonding π -bands removes the trigonal instability, as demonstrated by total energy calculations. In fact, while the Γ -point phonons of CaSi_2 in the AlB_2 structure show the presence of an instable phonon, in agreement with FLAPW total energy calculations, in CaBeSi the phonons are stable, as shown in Table I. Table I shows that this system has lower phonon frequencies than the diborides, as is normal

given the heavier atomic species involved. If we now imagine to vary x in $\text{CaBe}_x\text{Si}_{2-x}$, we will therefore have that, at some value of x , the B_{1g} mode, corresponding to the trigonal distortion, will be close to an instability. This situation may thus offer an interesting playground in the search for superconducting materials.

The Fermi level of CaBeSi cuts the σ bands, leaving hole pockets quite similar to those of MgB_2 . While it is difficult to say, on the basis of our electronic structure calculations only, whether the similarities with MgB_2 band structure can lead to superconductivity, it may be useful to provide hints on the stability of this compound, which may help experimentalists in the search for new compounds. The PDOS in Fig. 10 show a strong hybridization between Si and Be states, in the valence region. In other words, substitutions on the Si site can be possible without disrupting the sp^2 network if the one-electron energies of the impurity atoms are comparable with those of Si, and light atoms should be preferred in order to keep high values of phonon frequencies. We may suggest B, which however corresponds to a hole doping smaller than Be.

V. CONCLUSIONS

We have performed electronic structure calculations for MgB_2 , BeB_2 , $\text{Mg}_{0.5}\text{Al}_{0.5}\text{B}_2$, CaSi_2 in the trigonal and in the AlB_2 -type polymorphs at the high pressure experimental structural parameters, and for the $\text{CaBe}_x\text{Si}_{2-x}$ system ($x = 1$), experimentally stabilized for $x = 0.75$. We have calculated band structures, PDOS, transport properties and phonon frequencies, using the FLAPW and the norm-conserving ab-initio pseudopotential methods, within the local density approximation. The following conclusions can be drawn on the basis of our calculations: as compared to MgB_2 , BeB_2 has a similar filling of σ bands, but differs in terms of π states near E_F . The DOS at E_F is lower, and some phonon frequencies are substantially higher while others are comparable or lower. It would be interesting to further investigate this compound. Al substitution cannot be fully simulated by a rigid band model, as the π antibonding states appear to be quite sensitive to Al substitution, and absorb much of

the added electrons. Transport properties show a substantial two-dimensionality of these compounds, due to π states.

We studied CaSi_2 in its trigonal structure, and show that the distortion can be removed only by subtracting (in a virtual crystal-like approximation) at least 0.7 electrons. In fact, CaBeSi shows no tendency towards trigonal distortion, and electron states near E_F of similar bonding nature to those of MgB_2 .

VI. ACKNOWLEDGEMENTS

We thank M. Affronte and A. Gauzzi for stimulating discussions, and M. Affronte for sharing his results prior to publication. This work was partially supported by the Italian Consiglio Nazionale delle Ricerche (CNR) through the “Progetto 5% Applicazioni della superconduttività ad alta T_c ”.

TABLES

TABLE I. Theoretical structural parameters (in Å) and phonon frequencies at Γ (in cm^{-1}) for the AlB_2 type systems. Level degeneracies are shown in parenthesis.

	MgB2	BeB2	AlB2	CaBeSi
a	3.045	2.903	2.976	3.914
c	3.480	2.853	3.237	4.488
(2) E_{1u}	349	327	306	189
(1) A_{2u}	426	213	437	247
(2) E_{2g}	575	893	996	461
(1) B_{1g}	708	642	515	346

REFERENCES

- [1] J. Nagamatsu, N. Nakagawa, T. Muranaka, Y. Zenitani, and J. Akimitsu *Nature*, **410**, 63-64 (2001)
- [2] S. L. Bud'ko, G. Lapertot, C. Petrovic, C. E. Cunningham, N. Anderson, and P. C. Canfield, *Phys. Rev. Lett.* **86**, 1877 (2001)
- [3] J.S. Slusky, N. Rogado, K.A. Regan, M.A. Hayward, P. Khalifah, T. He, K. Inumaru, S. Loureiro, M.K. Haas, H. W. Zandbergen, R.J. Cava (cond-mat/0102262)
- [4] B. Lorenz, R. L. Meng, C. W. Chu (cond-mat/0102264)
- [5] I.I. Tupitsyn, *Sov. Phys. Solid State* **18**, 1688 (1976); R.C. Linton, *Thin Solid Film* **20**, 17 (1974); S.H. Liu, L. Kopp, W.B. England and H.W. Myron, *Phys. Rev. B* **11**, 3463 (1975).
- [6] I.I. Tupitsyn, I.I. Lyakovskaya, M.S. Nakhmanson, and A.S. Sukhikh, *Sov. Phys. Solid State* **16**, 2015 (1975).
- [7] D.R. Armstrong, A. Breeze, and P.G. Perkins, *J. Chem. Soc. Faraday Trans. I*, **73**, 952 (1977)
- [8] S. Massidda, Ph. D. thesis, ISAS-SISSA, Trieste (1985). S. Massidda and A. Baldereschi, unpublished. A. J. Freeman, A. Continenza, M. Posternak, and S. Massidda, in *Surface Properties of Layered Structures*, ed. G. Benedek, (Kluwer, Netherlands 1992).
- [9] S. Massidda, A. Baldereschi, *Solid State Commun.* **66**, 855 (1985).
- [10] T. Fauster, F.J. Himpsel, J.E. Fischer and E. W. Plummer, *Phys. Rev. Lett.* **51**, 430 (1983).
- [11] M. Posternak, A. Baldereschi, A.J. Freeman, and E. Wimmer, *Phys. Rev. Lett.* **52**, 863 (1984).

- [12] J. Kortus, I.I. Mazin, K.D. Belashchenko, V.P. Antropov, and L.L. Boyer, (cond-mat/0101446)
- [13] K.D. Belashchenko, M. van Schilfhaarde, and V.P. Antropov, (cond-mat/0102290).
- [14] J.E. Hirsch, (cond-mat/0102115)
- [15] P. Bordet, M. Affronte, S. Sanfilippo, M. Núñez-Regueiro, O. Laborde, G.L. Olcese, A. Palenzona, S. LeFloch, D. Levi, M. Hanfland Phys. Rev. B **62**, 11392 (2000).
- [16] S. Sanfilippo, H. Elsinger, M. Nunez-Reguerio, O. Laborde, S. LeFloch, M. Affronte, G.L. Olcese, and A. Palenzona, Phys. Rev. B **61**, R3800 (2000); P. Bordet et al. *ibid* **62**, 11392 (2000).
- [17] J.H. Weaver, A. Franciosi, V.L. Moruzzi, Phys. Rev. B **29**, 3293 (1979)
- [18] S. Fahy, and D.R. Hamann, Phys. Rev. B **41** 7587, (1990)
- [19] O. Bisi, L. Braichovic, C. Carbone, I. Lindau, A. Iandelli, G.L. Olcese, A. Palenzona, Phys. Rev. B **40**, 10194 (1989)
- [20] K. Kusakabe, Y. Tateyama, T. Ogitsu and S. Tsuneyumi, Rev. of High Pressure Sci. Technol. **7**, 193 (1998)
- [21] H.J.F. Jansen and A.J. Freeman, Phys. Rev. B **30**, 561 (1984); M. Weinert, H. Krakauer, E. Wimmer and A.J. Freeman, *ibid.* **24**, 864 (1981).
- [22] H.J. Monkhorst and J.D. Pack, Phys. Rev. B **13**, 5188 (1976).
- [23] D. Koelling, and J. H. Wood, J. Comput. Phys. **67**, 253, (1986) See also N. Hamada, S. Massidda, Jaejun Yu, A. J. Freeman, Phys. Rev. B **42**, 6238 (1990).
- [24] The ABINIT code is a common project of the Universite Catholique de Louvain, Corning Incorporated, and other contributors (URL <http://www.pcpm.ucl.ac.be/abinit>).
- [25] S. Baroni, P. Gianozzi, and A. Testa, Phys. Rev. Lett. **58**, 1861 (1987); N.E. Zein, Sov.

- Phys. Solid State **26**, 1825 (1984)
- [26] X. Gonze, Phys. Rev. B55, 10337 (1997) ; X. Gonze and C. Lee, Phys. Rev. B55, 10355 (1997).
- [27] N. Troullier, and J.L. Martins Phys. Rev. B 43, 1993 (1991)
- [28] S.G. Louie, S. Froyen and M.L. Cohen, Phys. Rev. B**26** 1738 (1982)
- [29] D.E. Sands, C.F. Cline, A. Zalkin, and C.L. Hoenig, Acta Cryst. **14**, 309 (1961). After the first submission of this paper, experimental measurements by I. Felner (cond-mat/0102508) give an average lattice constant, in agreement with Sands et al., but do not find any superconducting transition down to 5 K. A later report by D.P. Young, P.W. Adams, J.Y. Chan, and F.R. Fronczek, on the other hand, reports a complex crystallographic structure for BeB_{2.75}, superconducting at about 0.7 K.
- [30] Our results are in very good agreement with those reported by Y. Kong, O.V. Dolgov, O. Jepsen, and O.K. Andersen, (cond-mat/0102499), and by K.-P. Bohnen, R. Heid, and B. Renker, (cond-mat/0103319), after the first submission of the present manuscript.
- [31] W. N. Kang, C. U. Jung, Kijoon H. P. Kim, Min-Seok Park, S. Y. Lee, Hyeong-Jin Kim, Eun-Mi Choi, Kyung Hee Kim, Mun-Seog Kim, Sung-Ik Lee, (cond-mat/0102313).
- [32] from *Inorganic crystal structure database* N.V. Vekshina, L.Y. Markovskii, Y.D. Kondrashew, and T.K. Voevodskaya, Zhurnal Prikladnoi Khimii Z. P. K.H.A., **44**, 970 (1971)
- [33] W.B. Pearson, *Handbook of Lattice Spacing and Structures of Metals and Alloys*(Pergamon, New York, 1958)
- [34] M. Affronte, O. Laborde, G.L. Olcese and A.Palenzona, J. of alloys Compounds **274** (1998) 68-73
- [35] J. Evers, J. Solid State Chem. **28**,369 (1979)

- [36] H. Nakano and S. Yamanaka, *J. Solid State Chem.* **108**, 260 (1994), and references therein.
- [37] from *Inorganic crystal structure database* N. May, W. Muellery, H. Schaefer, *Zeitschrift fuer Naturforschung, Teil B. Anorganische Chemie, Organische Chemie* **2**, 1947 (1977).

FIGURES

FIG. 1. Band structure of MgB₂. All the energies are referred to the Fermi level, taken as zero.

FIG. 2. Total and partial density of states (PDOS) for MgB₂.

FIG. 3. Band structure of BeB₂.

FIG. 4. Transport properties of MgB₂ and BeB₂ as a function of doping in a rigid band scheme. Full and dashed lines correspond to BeB₂ and MgB₂ respectively. Circles (squares) indicate the x, y (z) principal values of the plasma frequency Ω_p (in eV), of the mean squared Fermi velocity v_F (in 10^7 cm/sec) and of R_{xyz} (in 10^{-10} m³/C, notice that $R_{zxy} = R_{yzx}$). DOS are in states/eV-cell.

FIG. 5. Band structure of MgB₂ (panel (a)) and Mg_{0.5}Al_{0.5}B₂ at the experimental (panel (b)) and frozen MgB₂ (panel(c)) lattice parameters.

FIG. 6. Band structure of CaSi₂ in the ideal AlB₂ (dashed lines) and trigonal (full lines) structures .

FIG. 7. Total and partial density of states (PDOS) for CaSi₂ in the AlB₂ (dashed lines) and in the trigonal structure (full lines).

FIG. 8. Upper pannel: total energy of CaSi₂ as a function of the internal parameter z , for two different values of pressure, at the corresponding experimental lattice constants ($a = 3.7554$ Å, $c = 4.3951$ Å for $P = 15.0$ GPa and $a = 3.7668$ Å, $c = 4.4752$ Å for $P = 12.8$ GPa, after [15]). The experimental values of z are indicated by arrows. Lower pannel: same as above, at the larger experimental pressure (19.3 GPa), with Ca substituted by a virtual cation having nuclear charge $Z = 20 + x$. The experimental lattice parameters are $a = 3.708$ Å and $c = 4.028$ Å, $z = 0.448$). The zero of energy corresponds to the AlB₂ value $z = 0.5$.

FIG. 9. Band structure of $\text{CaBe}_x\text{Si}_{2-x}$ ($x = 1$) in the hexagonal Brillouin zone, at experimental lattice parameters.

FIG. 10. Total and partial density of states (PDOS) for $\text{CaBe}_x\text{Si}_{2-x}$ ($x = 1$) in the AlB_2 structures (see text).

Fig. 1 G. Satta et al.

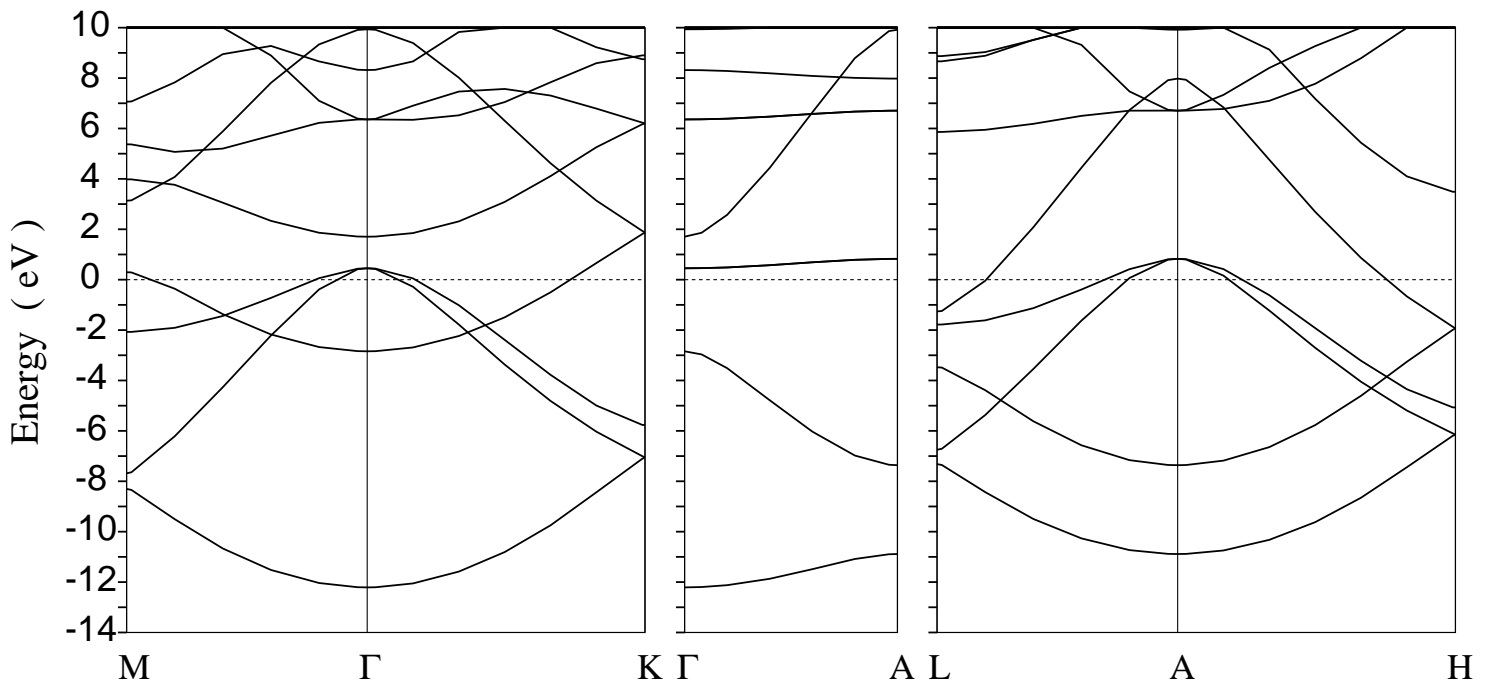
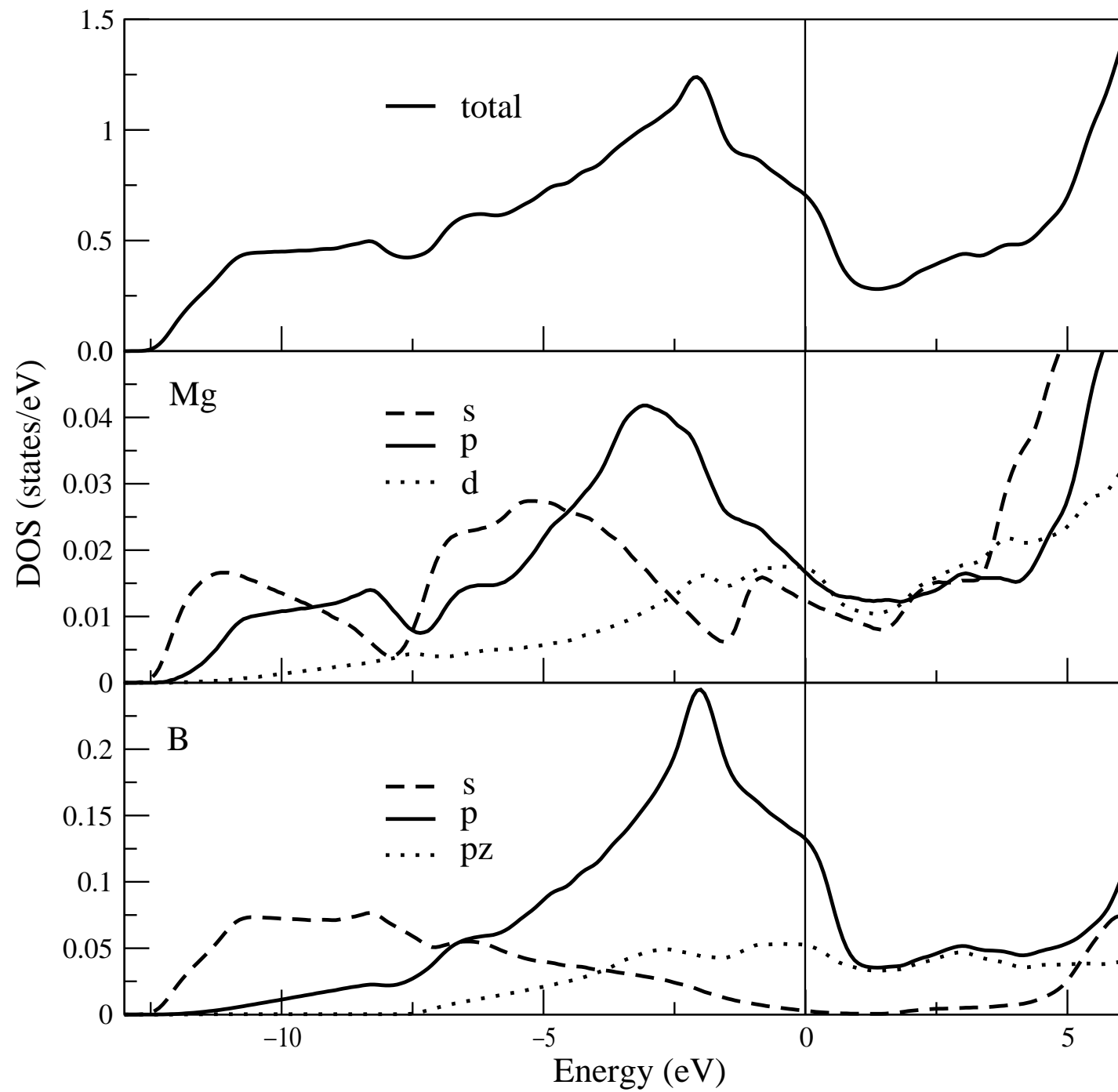


Fig. 2 G. Satta et al.



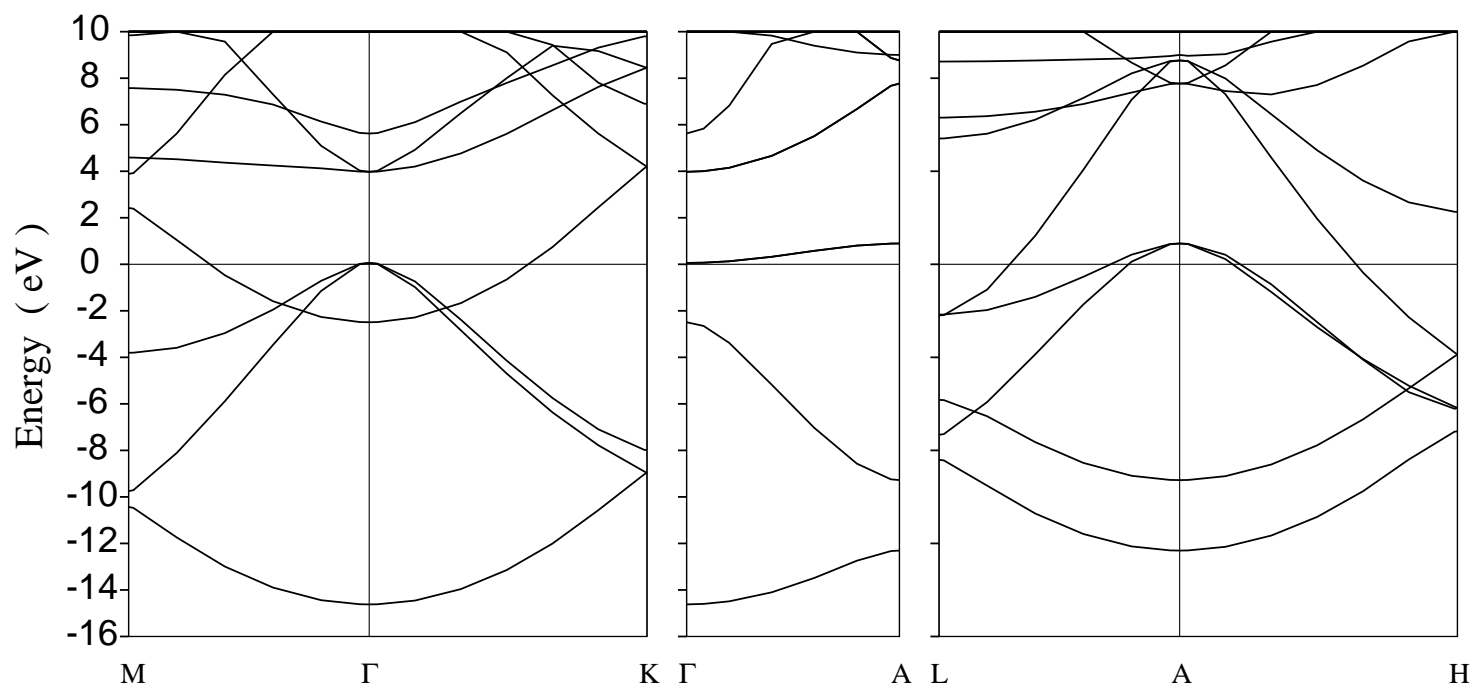


Fig. 3 G. Satta et al.

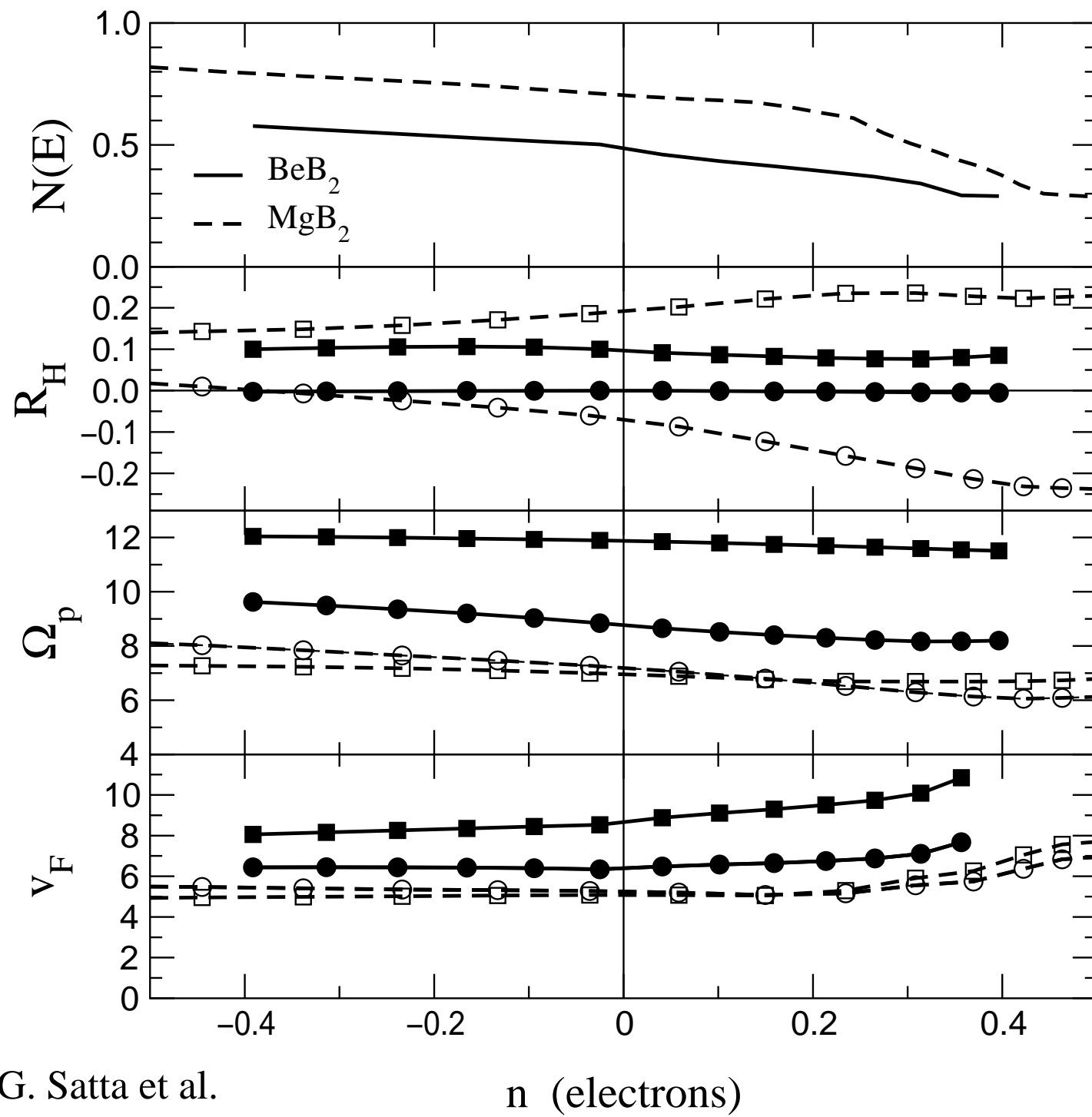
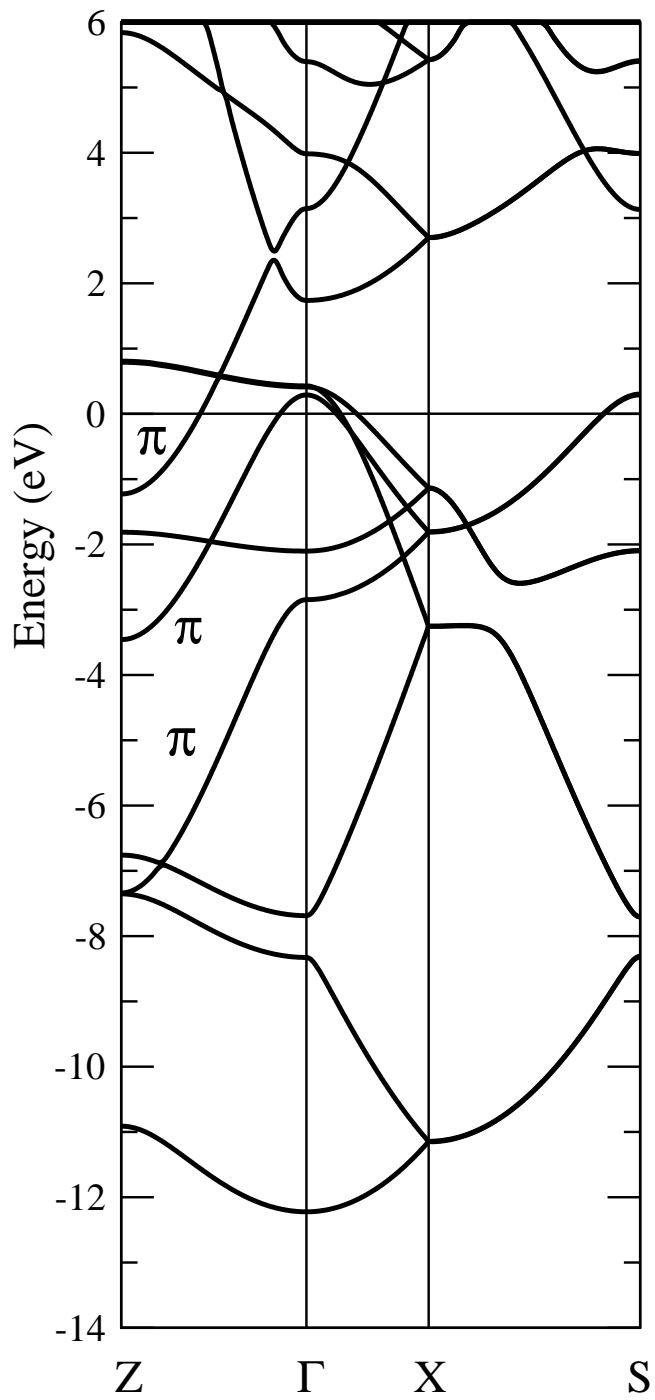
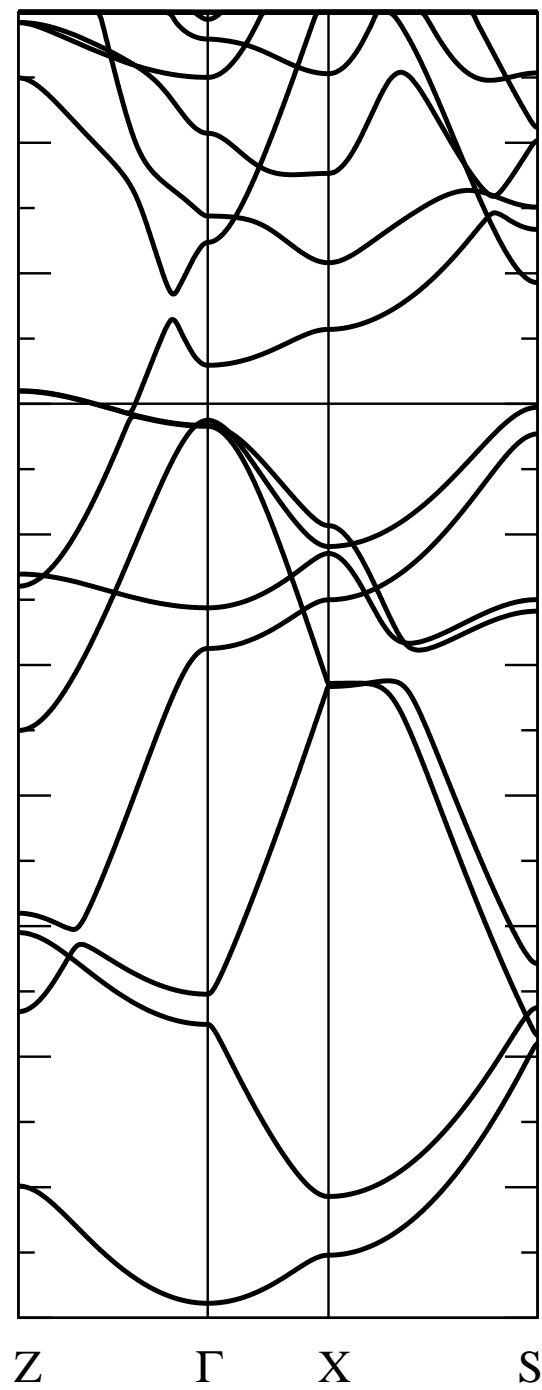


Fig. 4 G. Satta et al.

(a)



(b)



(c)

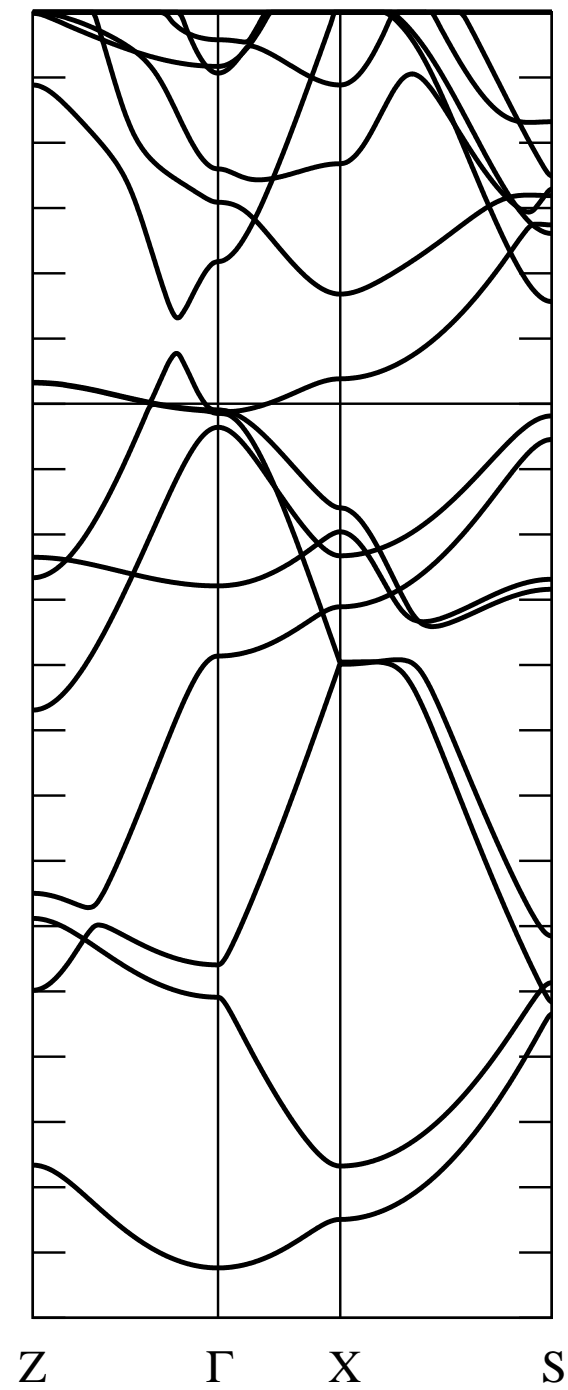
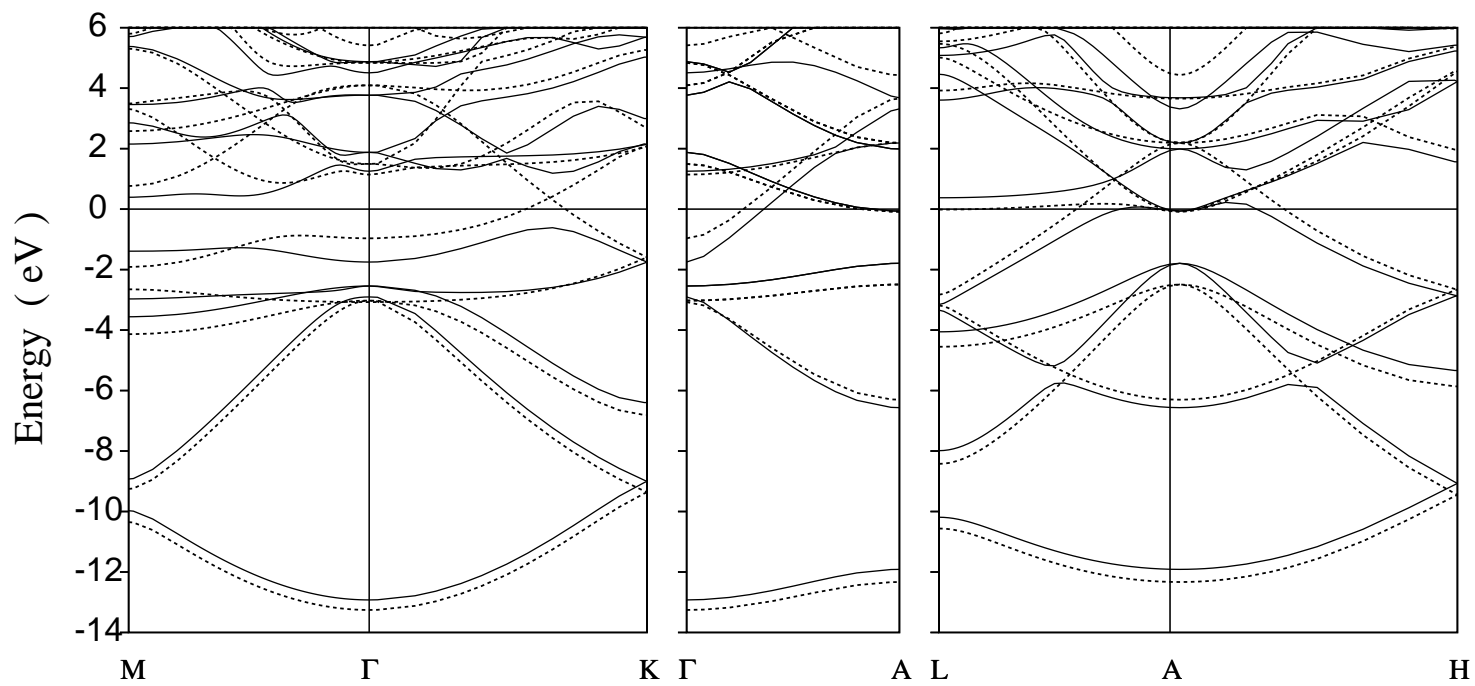


Fig. 5 G. Satta et al.

Fig. 6 G. Satta et al.



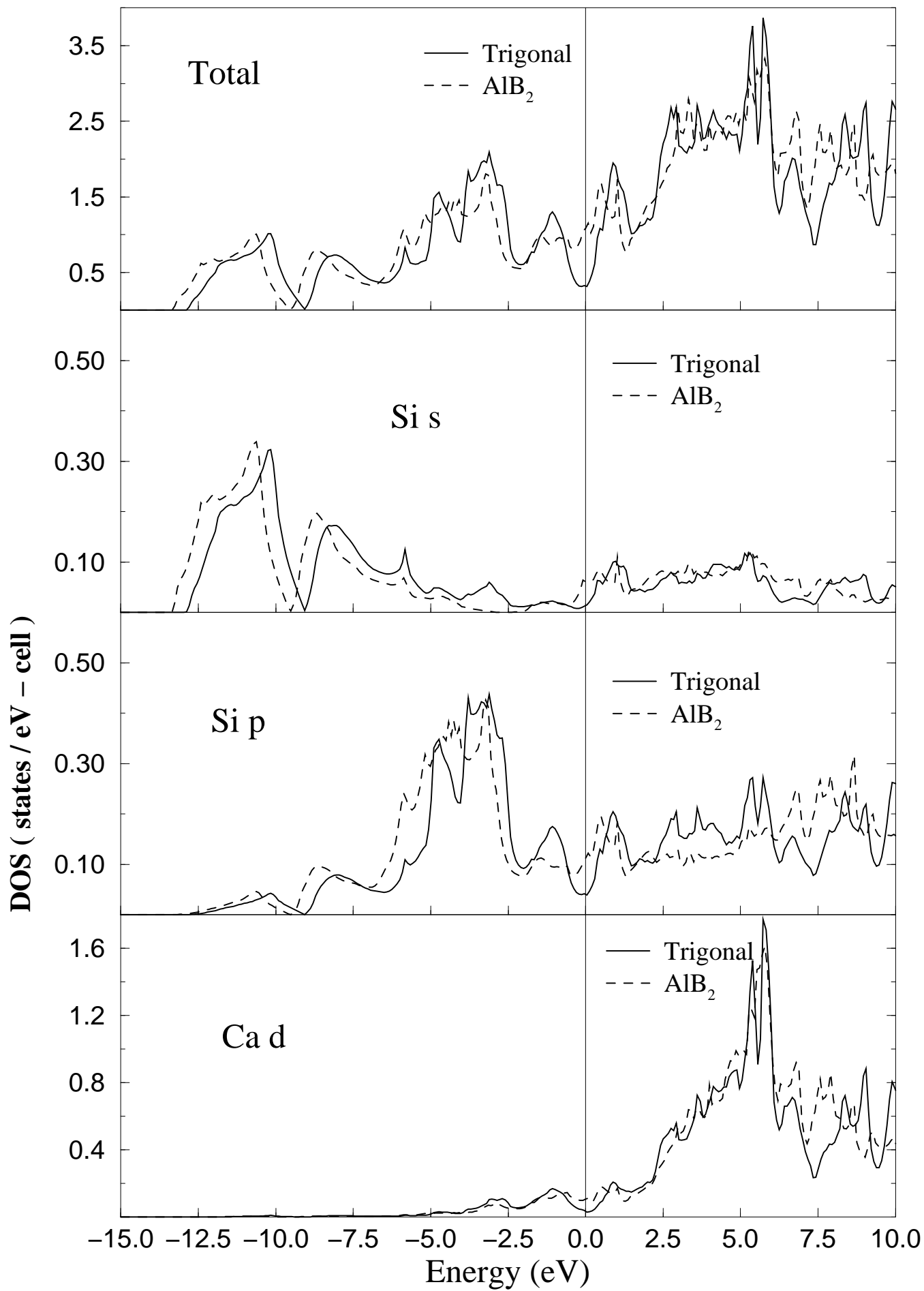


Fig. 7 G. Satta et al.

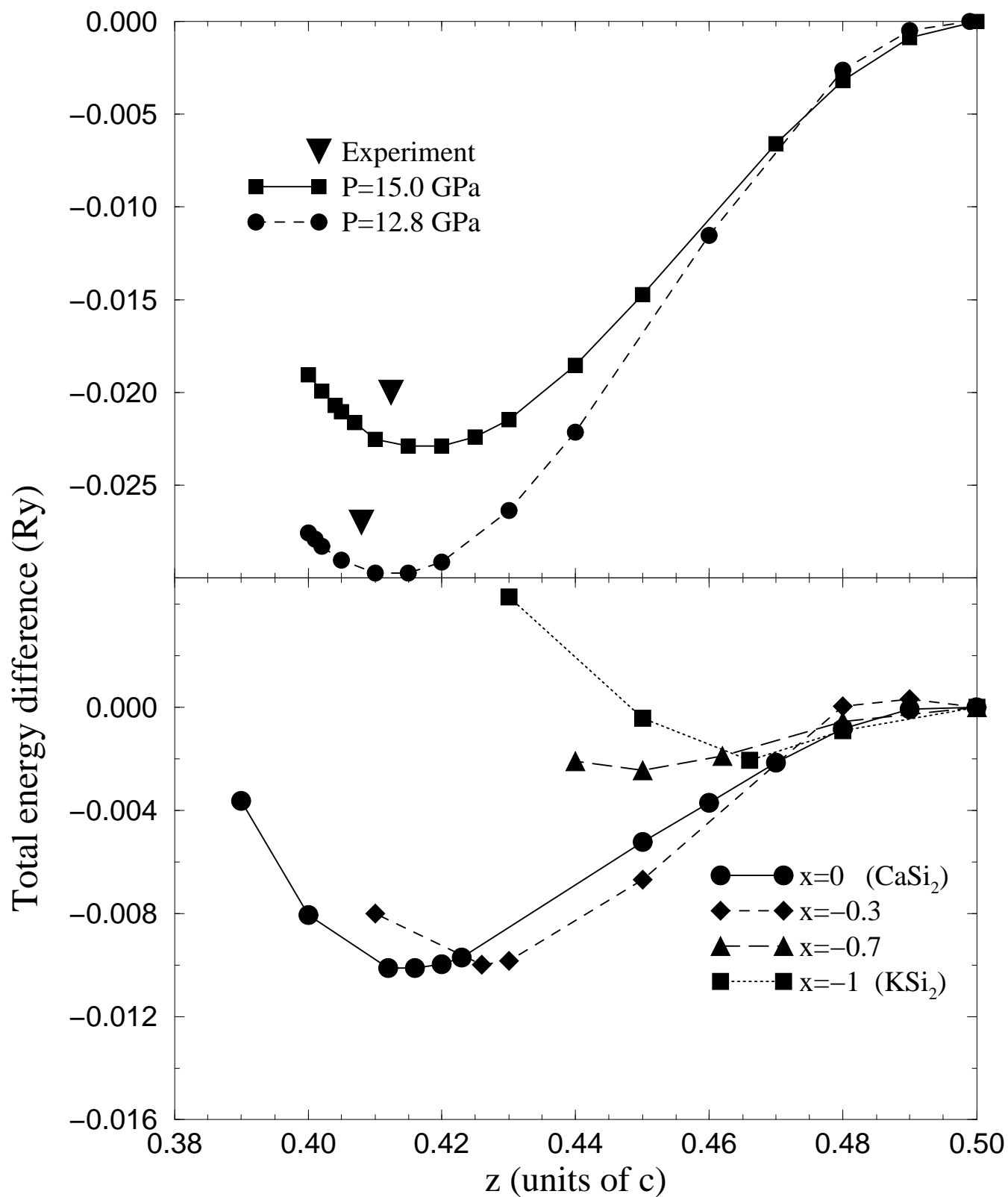
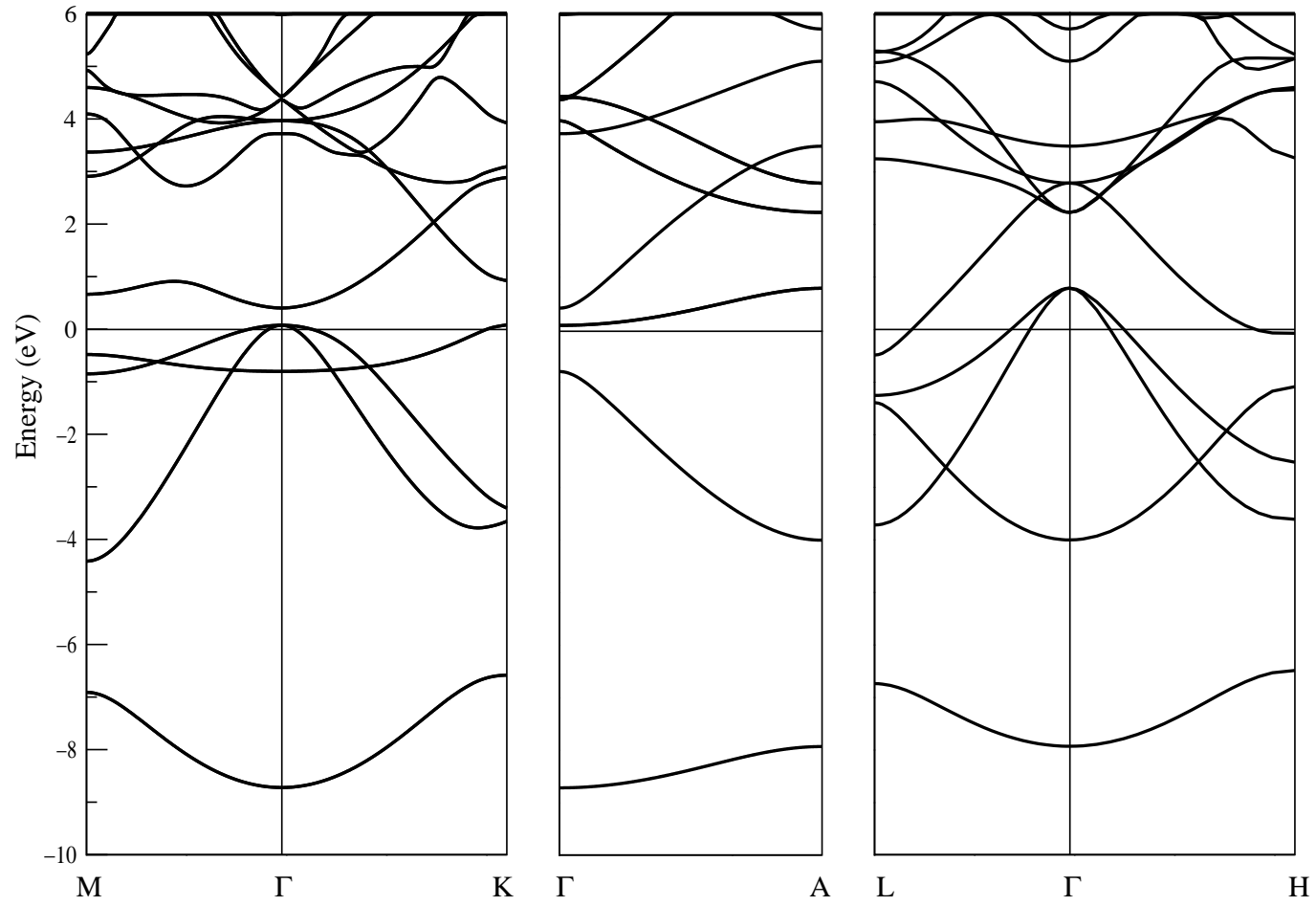


Fig. 8 G. Satta et al.

Fig. 9 G. Satta et al.



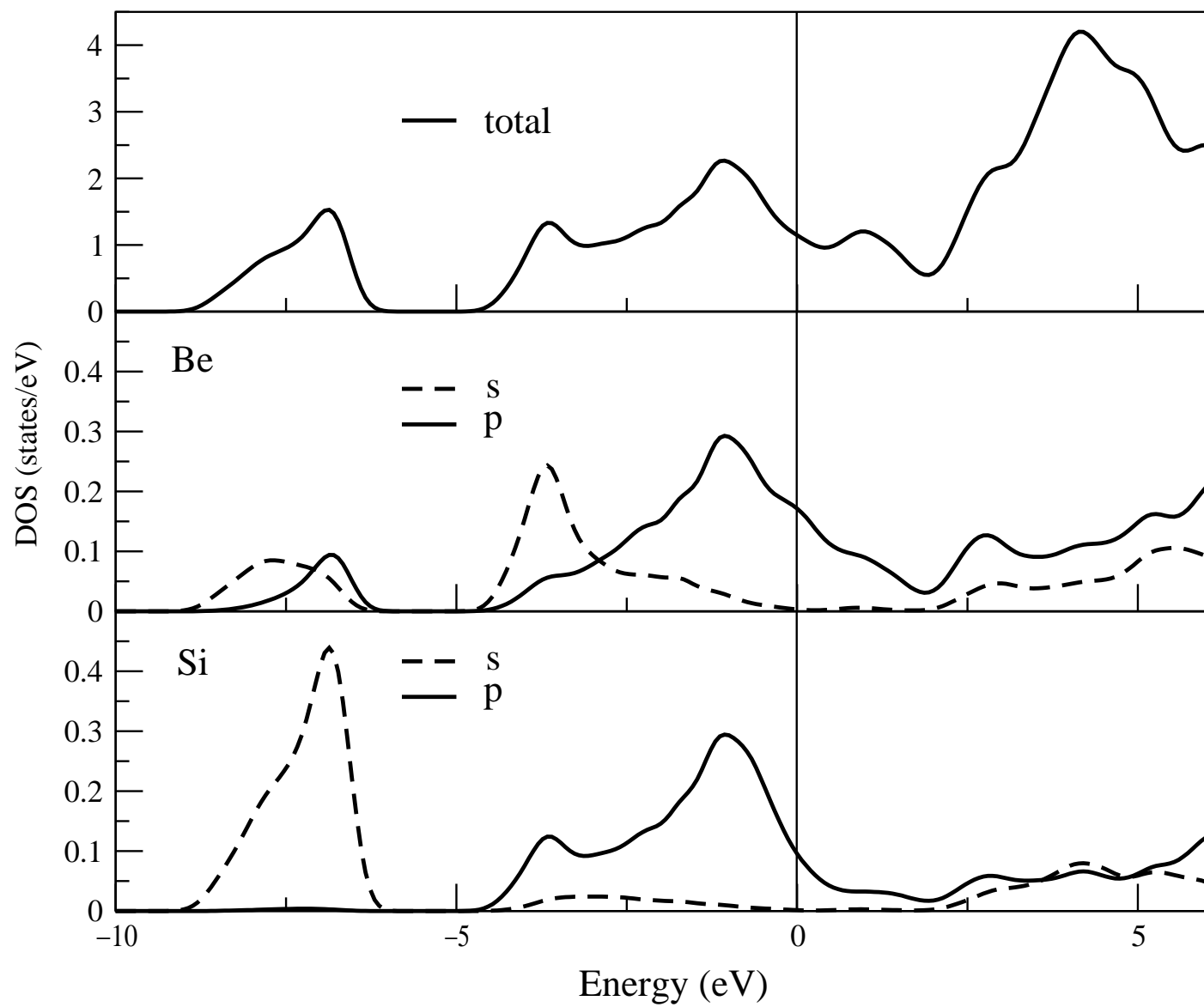


Fig. 10 G. Satta et al.